PAPER

The inhibitory effects of platinum(II) complexes on amyloid aggregation: a theoretical and experimental approach†

Sara La Manna,[a] Valentina Roviello,[b] Vittoria Monaco,[c,d] James A. Platts,[e] Maria Monti,[c,d] Elisabetta Gabano, [ID][f] Mauro Ravera [ID][g] and Daniela Marasco [ID]*[a]

Platinum (Pt)(II) square planar complexes are well-known anticancer drugs whose Mechanism of Action (MOA) are finely tuned by the polar, hydrophobic and aromatic features of the ligands. In the attempt to translate this tunability to the identification of potential neurodrugs, herein, four Pt(II) complexes were investigated in their ability to modulate the self-aggregation processes of two amyloidogenic models: Sup35p$_{7-13}$ and NPM1$_{264-277}$ peptides. In particular, phenanthriplatin revealed the most efficient agent in the modulation of amyloid aggregation: through several biophysical assays, as Thioflavin T (ThT), electrospray ionization mass spectrometry (ESI-MS) and ultraviolet-visible (UV-vis) absorption spectroscopy, this complex revealed able to markedly suppress aggregation and to disassemble small soluble aggregates. This effect was due to a direct coordination of phenanthriplatin to the amyloid, with the loss of several ligands and different stoichiometries, by the formation of $\pi-\pi$ and $\pi-$cation interactions as indicated from molecular dynamic simulations. Presented data support a growing and recent approach concerning the repurposing of metallodrugs as potential novel neurotherapeutics.

Introduction

Transition metal coordination compounds have unique and distinctive features including variable oxidation states, diverse range of geometries, coordination numbers and ligands.[1] A vast library of metal complexes was designed and explored over many years for diverse therapeutic applications in the field of cancer, microbial and viral infections, diabetes and neurodegenerative diseases (NDDs)[2] and many studies out-

[a]*Department of Pharmacy, University of Naples Federico II, 80131 Naples, Italy. E-mail: daniela.marasco@unina.it; Tel: +39-081-2532043*

[b]*Department of Chemical, Materials, and Industrial Production Engineering (DICMaPI), University of Naples Federico II, 80125 Naples, Italy*

[c]*Department of Chemical Sciences, University of Naples Federico II, 80126 Naples, Italy*

[d]*CEINGE Biotecnologie Avanzate "Franco Salvatore" S.c.a r.l., 80131 Naples, Italy*

[e]*School of Chemistry, Cardiff University, Park Place, Cardiff, CF10 3AT, UK*

[f]*Dipartimento per lo Sviluppo Sostenibile e la Transizione Ecologica, University of Piemonte Orientale, Piazza S. Eusebio 5, 13100 Vercelli, Italy*

[g]*Department of Sciences and Technological Innovation, University of Piemonte Orientale, Viale Michel 11, 15121 Alessandria, Italy*

†Electronic supplementary information (ESI) available: SEM micrographs of NPM1$_{264-277}$ + **1**, at 1:5 ratio, at 1 mm, and 300 μm; time evolution of RMSD relative to initial extended structure; time evolution of secondary structure in metal-free monomer and dimer MD simulation; deconvolution of CD spectra; bonded parameters from MCPB.py for **2** bound to Cys[12]. See DOI: https://doi.org/10.1039/d3dt02187d

lined that coordination chemistry plays a crucial role in the definition of the mechanisms of action (MOAs) of metallodrugs. MOAs generally depend on both the binding preferences of transition metals for biomolecules and the regulation of ligands exchanges with functional groups coming from proteins and oligonucleotides.[3] In spite of deep clinical diversity, NDDs share several events as the cellular accumulation of intrinsically disordered proteins and the dysregulation of the homeostasis of several metal ions in the brain, and, till now, no definite cures are available for these disorders, even if considerable advances in understanding the molecular mechanisms at the basis of these diseases and in the development of therapeutics have been carried out.[4]

The self- or hetero-assembly of amyloidogenic systems, as the Aβ-amyloid (Amyloid beta (Aβ or Abeta)), α-synuclein, huntingtin, tau and islet amyloid polypeptides, to form oligomers and fibrils is directly linked to NDDs as Alzheimer's, Parkinson's, and Huntington's diseases, frontotemporal dementia and type II diabetes.[5] Often the structural details of the oligomers/fibers formed by full-length proteins are elusive and very difficult to study, while, the investigations of the self-assemblies of protein fragments, as model, allow to deepen structural, biophysical and biological properties of *in vivo* amyloids.[5]

In the context of drug discovery processes in early steps of amyloid aggregation, metallodrugs can be employed. After the

pioneering study of Barnham *et al.*[6] many Pt complexes were investigated for their inhibitory properties of amyloid aggregation:[7] examples can be traced back to complexes containing heteroaromatic ligands such as pyridine or its derivatives,[8] imidazole,[9] thiazole, pyrazoles, quinoline and isoquinoline, tetrazoles and triazoles.[10] In detail, phenanthroline(phen)-Pt(II) complexes with two monodentate ligands exhibited inhibitory effects toward the aggregation of $A\beta_{1-40}$[11] and prion protein (PrP) fragments.[12] The inhibition mechanism depends on multiple factors as the coordination of the metal center, the 1st and 2nd electrostatic spheres around the ion, hydrogen bond networks and van der Waals interactions. Examples of multifactorial amyloid inhibition are several Co-[13] and Pt-compounds[14] bearing polyaromatic ligands: they demonstrated reduction of Aβ aggregation through a coordinative mechanisms aided by the formation of π–π stacking interactions with aromatic side chains.[15] Two glycoconjugate pentacoordinate Pt-complexes were analyzed in their capacity to affect the self-aggregation processes of two fragments of the C-terminal region of Aβ-peptide, $A\beta_{21-40}$ and $A\beta_{25-35}$. The water-soluble complex, named $1Pt_{dep}$, inhibited the aggregates through the direct binding to Aβ-peptides, drastically reducing the morphological amyloid features of fibers.[16]

On the basis of these promising results, herein we investigated the ability of four Pt(II) complexes to modulate the aggregation of two amyloid models, $NPM1_{264-277}$ and $Sup35p_{7-13}$, whose sequences are reported in Table 1. In the screening of agents able to modulate amyloid aggregation, often protein/peptide, even if not directly involved in neurodegeneration, are employed as models of amyloids. This is the case of Nucleophosmin 1 (NPM1), which is not an amyloid protein strictly speaking, but presents an amyloid-prone fragment, including 264–277 residues.[17] In the recent past, we tested the ability of several metal-based CORM (carbon monoxide releasing molecules) to modulate the amyloid aggregation $NPM1_{264-277}$.[18,19] Conversely, the heptapeptide GNNQQNY, spanning residues 7–13 of the Yeast Prion Protein Sup35p ($Sup35p_{7-13}$), is directly involved in the aggregation of Sup35p since it is located in the prion-determining N-terminal domain (PrD),[20] which demonstrated able to form amyloid fibrils.[21,22]

In a recent study, we have investigated the ability of a series of square planar Pt(II)-complexes to inhibit the aggregation of amyloid peptides. The pyridine-based cationic, $[PtCl(tpy)]^+$, called Pt-terpy, exhibited good inhibitory effects and the ability to reduce the cytotoxicity of amyloid in human SH-SY5Y neuroblastoma cells.[23] To deepen the MOAs of similar compounds, in the present study we investigated the effects of square planar Pt(II) complexes differing in their charge: positive for two complexes and neutral for other two compounds. In

detail, we analyzed the (SP-4-3)-diamminechlorido (quinoline) platinum(II) nitrate (quinoplatin, **1**) and (SP-4-3)-diamminechlorido(phenanthridine)platinum(II) nitrate (phenanthriplatin, **2**)[24] and the enantiomeric (SP-4-2)-dichlorido(1,1′-binaphthalene-2,2′-diamine)platinum(II), **3R** and **3S**, respectively (Fig. 1). These complexes contain a chiral ligand (*i.e.*, 1,1′-binaphthalene-2,2′-diamine, DABN) and the R isomer demonstrated to interact with the G-quadruplex structure $AG_3(TTAGGG)_3$ less efficiently than its S counterpart.[25–27]

The ability of Pt(II) complexes to interfere with the aggregation of amyloid models was investigated *via* a range of spectroscopic and biophysical techniques as wells as by molecular dynamic (MD) studies.

Experimental section

Peptide synthesis

Peptides were synthesized as already reported.[19] both in the acetylated and amidated form. The sequences are reported in Table 1, after purification they were lyophilized and treated with HFIP to ensure a monomeric state and then stored at −20 °C until use.

Synthesis of complexes

Complexes **1–3** were synthesized according to literature procedures. Briefly, (SP-4-2)-diamminedichloridoplatinum(II), cisplatin, was reacted with $AgNO_3$ in DMF to remove one chloride ion, then the N-heterocyclic ligand was added in a 1 : 1 molar ratio and the reaction was stirred for 16 h at 55 °C. The following purification steps gave **1** and **2** as white solids (yield: 70% and 59% for **1** and **2**, respectively).[26] Complexes **3R** and **3S** were synthesized directly by reacting equimolar quantities of K_2PtCl_4 and the R- or S-isomers of 1,1′-binaphthalene-2,2′-diamine (DABN) in DMF at 40 °C in the dark overnight. The following purification steps gave **3R** and **3S** as yellow solids (yield: 78% and 72% for the R and S-isomers counterparts,
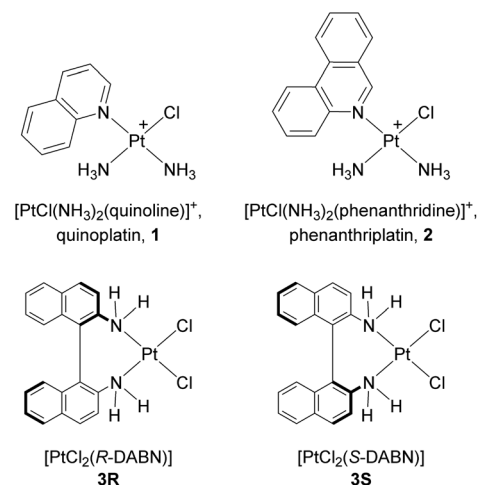
Table 1 Amyloid sequences analyzed in this study

Peptide	Sequence
$NPM1_{264-277}$	Ac-VEAKFINYVKNCFR-NH₂
$Sup35p_{7-13}$	Ac-GNNQQNY-NH₂

Fig. 1 Structure of the Pt(II) complexes investigated in the present work; DABN = 1,1′-binaphthalene-2,2′-diamine.

respectively).[26] The stabilities of Pt complexes were already reported in ref. 25–27

Fluorescence assays

ThT assay was carried out on fluorescence reader Envision 2105 (PerkinElmer) in black plates (96 well) under stirring. Measurements were collected every 2 min (λ_{ex} 440 nm and λ_{em} 483 nm). Assays were performed at 25 °C employing a peptide concentration of 100 μM for $NPM1_{264-277}$ and 400 μM for $Sup35_{7-13}$ in 50 mM borate (pH 8.5) and 50 mM phosphate buffer (pH 7.4) respectively, for both a ThT final concentration of 50 μM. Pt-complexes stock solutions (50 mM in water for **1**, 10 mM in water for **2** and 50 mM in DMSO for **3R** and **3S**) were opportunely diluted to obtain employed ratios with respect to amyloid peptides. Disaggregation assays were performed on a Jasco FP 8300 spectrofluorometer (JASCO, Tokyo, Japan) in a 1 cm cuvette under magnetic stirring (λ_{ex} = 440 nm, λ_{em} = 483 nm). Spectra were recorded every 15 min and assays were performed in duplicates, and intensities were reported as averaged values and transformed as percentages of aggregated fraction. Indicating F_{max} as the maximum reached fluorescence signal and n is a cooperativity parameter $t_{1/2}$ value is the time at which F is equal to one-half of F_{max} through the fitting of the data of F versus time through the empirical Hill equation as follows:

$$F(t) = F_{max} \frac{\left(\frac{t}{t_{\frac{1}{2}}}\right)^n}{1 + \left(\frac{t}{t_{\frac{1}{2}}}\right)^n}$$

UV-vis absorption spectroscopy

UV/vis titrations of Pt-complexes with $NPM1_{264-277}$ were carried out employing a BioDrop Duo UV Visible Spectrophotometers (Cambridge, United Kingdom). To a fixed concentration of the Pt(II) complexes (50 μM). Repeated additions of 1.25 μL of $NPM1_{264-277}$ stock solution (2 mM) in water, kept at 0 °C, were performed till reaching a ratio of 1 : 2.5 complex : $NPM1_{264-277}$. Spectra were registered in the 250–500 nm range, upon each addition. For **2**, EC_{50} value was derived from non-linear regression of the data employing log [inhibitor] vs. response and "dose–response stimulation equation" of GraphPad program.

Circular dichroism

CD spectra of $NPM1_{264-277}$ (100 μM) in 10 mM borate buffer pH 8.5, alone or at 1 : 1 molar ratio with metal complexes, were registered on a Jasco J-815 spectropolarimeter (JASCO, Tokyo, Japan), at 25 °C using a 0.1 cm path-length quartz cuvette. Deconvolutions of CD spectra were obtained by BESTSEL software (**https://bestsel.elte.hu/**).

ESI-MS analysis

$NPM1_{264-277}$ at 5 μM in 15 mM AMAC (Ammonium acetate) buffer pH = 7.0, was incubated at two different times (0 and 4 h) with 1 : 5 ratios with **2** compound and the obtained mixtures were analyzed by native ESI-MS on a Q-ToF Premier (Waters, Milliford, MA, USA) mass spectrometer. The analyses were carried out by direct injection at 10 μL min^{-1}, setting the source parameters at 3 kV for capillary voltage and 42 kV for cone voltage. The acquisition range was scanned from 100 to 2000 m/z in 1 s and the raw data were processed with MassLynx 4.1 software (Waters, Milliford, MA, USA). Fosforic acid solution at 50% (v/v) in acetonitrile was used for the instrument calibration.

Scanning electron microscopy

Samples (100 μL) containing $NPM1_{264-277}$ (100 μM) alone or mixed with Pt-complexes at a 1 : 5 ratio, at two different times of aggregation (t 2 h for **3S** and 4 h for **1** and **2**), were dropped on stubs and introduced into chamber of field emission scanning (Nova NanoSem 450 FEI/ThermoFisher Scientific), to obtain SEM micrographs at 3.00 and 5.00 kV in high vacuum mode, with an Everhart Thornley Detector (ETD) and the Through the Lens Detector (TLD).

Computational methods

The structure of $NPM1_{264-277}$ was built in extended ($\varphi = \psi = 180°$) form and capped with amide groups. Its geometry was optimised at GFN2-xTB level in implicit model of water, in the xtb package. Potential Pt binding sites were explored by manually attaching **2** to different polar atoms in backbone and side chains, followed by an optimisation at the same level. Optimized geometries were imported into Amber16 [28] using the tleap utility, assigning parameters for the ff14SB[29] forcefield in GBSA implicit model of aqueous solvation. For Pt-bound peptide, parameters for metal, ligands and bound Cys were obtained using the MCPB.py[30] approach, in which bonded parameters were extracted from DFT calculations using the Seminario method,[31] while non-bonded parameters were taken from RESP calculations. These were combined with ff14SB for proper comparison with metal-free simulations, and key data are reported in the Table S2.† All systems were minimised with 1000 steps of steepest descent. Three independent MD trajectories were then generated, first by heating to 300 K over 1 ns with a further 1 ns equilibration, both with positional restraints on all atoms, then with 100 ns of unrestrained MD. RMSD data (ESI Fig. S1†) indicate that stable trajectories were established within a few ns. Analysis of all 300 ns of trajectory data was performed using cpptraj,[25] concentrating on secondary structure and clustering: the latter using a k-means approach with 10 clusters.

Results and discussion

Pt(II) complexes interfere with amyloid aggregation

To analyze the effects of Pt-compounds on the self-recognition process of amyloid systems, Thioflavin T (ThT) binding assay was employed;[32] and both inhibitory (Fig. 2) and disaggregating (Fig. 3) experiments were carried out. The time courses of the ThT fluorescence of $NPM1_{264-277}$ and $Sup35p_{7-13}$ peptides
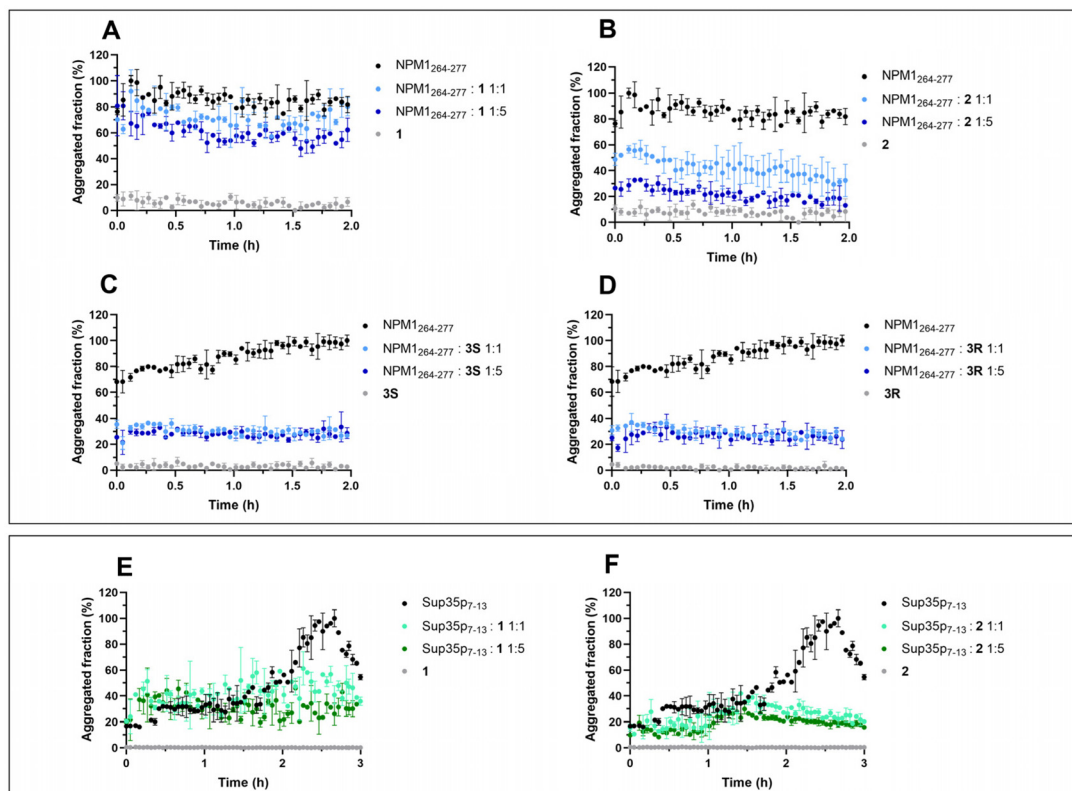
Fig. 2 Inhibitory effects of Pt-complexes on amyloid aggregation. Time course of ThT fluorescence emission intensity, reported as % of aggregated fraction, of NPM1$_{264-277}$ (upper panel) and Sup35p$_{7-13}$ (lower panel) upon incubation with: (A and E) **1**; (B and F) **2**; (C) **3S**; (D) **3R** at 1 : 1 and 1 : 5 peptide to Pt compound ratios.
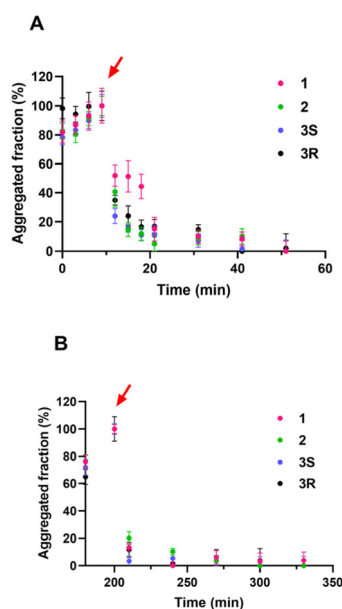

Fig. 3 Disaggregation effects of Pt-complexes **1–3**. Percentage of aggregated fraction, for NPM1$_{264-277}$ (A) and Sup35p$_{7-13}$ (B) before and after the addition of Pt complexes **1–3** at 1 : 5 ratio. The addition of Pt-complexes is indicated by an arrow.

alone and incubated with complexes are reported in Fig. 2; two peptide : Pt-complex molar ratios were analyzed, 1 : 1 and 1 : 5. For NPM1$_{264-277}$, in the absence of complexes, the starting value of fluorescence was different from 0 for an immediate partial oligomerization during sample preparation[17] (Fig. 2A and B) and the time intervals required to reach saturated ThT signal appeared fast, ~10 min, while a slight delay is observed, ~1.5 h, for the presence of DMSO (Fig. 2C and D) that is the control condition required for compounds **3R** and **3S**. From the comparison of time-course profiles, all complexes were able to inhibit the aggregation of NPM1$_{264-277}$ even if to different extents: between the charged complexes, the most effective inhibitor was found to be complex **2**, since it inhibited NPM1$_{264-277}$ aggregation of ~50% at 1 : 1 and ~70% at 1 : 5 ratio (Fig. 2B), whereas the inhibitory effect of **1** was significantly less at both ratios (Fig. 2A). Unlike **1** and **2**, no difference in the inhibition effects of **3R** and **3S** was detected that was of ~50%; for both compounds in both ratios (Fig. 2C and D).

By comparing aggregation times of NPM1$_{264-277}$ and Sup35p$_{7-13}$ peptides alone, great differences are observable: indeed in the case of Sup35p$_{7-13}$, the time of the half reduction of the signal in the amyloid growth phase, named $t_{\frac{1}{2}}$, was evaluated of ~2.5 h (Fig. 2E and F). Noticeably the sudden decrease of folded fraction after ~2.5 h is likely due formation of less soluble species. Thus, differently from NPM1$_{264-277}$,

these features hamper performance of inhibitory assays with **3R** and **3S** complexes which are stable for only two hours.[26] Consequently, the effects of only complexes **1** and **2** preincubated with Sup35p$_{7-13}$ were evaluated. Compound **1** appeared almost ineffective while **2** showed an inhibition of ~75% (Fig. 2E and F), at both molar ratios. No interference signals with ThT were observed for all complexes for the entire durations of the analyses.

Having assessed the different abilities of metal complexes to suppress amyloid aggregation, we evaluated if they are also able to disaggregate soluble pre-formed oligomers,[33] monitoring the ThT signals after the addition of metal compounds to NPM1$_{264-277}$ and Sup35p$_{7-13}$ aggregates at 1 : 5 ratio (Fig. 3). On the basis of different aggregation kinetics (see above), Sup35p$_{7-13}$ was pre-aggregated in the absence of the complexes for 3 hours, while NPM1$_{264-277}$, which is partially aggregated at t = 0, was allowed to further aggregate for 10 min before starting experiments. Upon the addition of Pt-complexes to both amyloids, a decrease in ThT fluorescence intensity was observed with a greater effect of **2** with respect to **1**. Indeed, while the addition of **1** caused a disaggregating effect on NPM1$_{264-277}$ and Sup35p$_{7-13}$ of 30% and 60%, respectively, **2** showed a stronger effect by inducing a reduction of 40% and 70%, respectively. Also the neutral complexes **3R** and **3S** showed a strong disaggregating capacity that led to a reduction of ThT signal of ~60% for NPM1$_{264-277}$ and 45% for Sup35p$_{7-13}$.

On the basis of similar effects of Pt-complexes observed on NPM1$_{264-277}$ and Sup35p$_{7-13}$, we focused only on NPM1$_{264-277}$, since its longer sequence with respect to the heptapeptide Sup35p$_{7-13}$, makes it more sensitive in subsequent conformational studies. ThT results indicated similar inhibitory effects provided similar inhibitory effects, hence we continued with compounds **1** and **2** which demonstrated more stable during time.[26]

To assess whether observed inhibitory effects of Pt-complexes could be accompanied by variations of ligands' field around metal center, changes in the UV-vis absorption spectra[34–37] were evaluated, upon the addition of NPM1$_{264-277}$ to aqueous solutions of **1** and **2** at a fixed concentration. These experiments, reported in Fig. 4, confirmed different behaviors for **1** and **2**. In fact, the titration with NPM1$_{264-277}$ of **2** (Fig. 4B) exhibited marked variations of intensity of several absorption bands. In detail the LMCT band at 311 nm (ref. 37) provided saturated values of absorbance at 1 : 2.5 complex : peptide ratio and an estimation of EC$_{50}$ (half-maximal effective concentration) of 26 ± 3 μM (inset of Fig. 4B). On the contrary, the same experiments carried out for **1** did not show significant variations of absorbances at 309 nm (Fig. 4A).

Charged Pt-complexes stabilize the β-conformation of NPM1$_{264-277}$

To gain insights into effects of Pt-complexes on the NPM1$_{264-277}$ conformation, circular dichroism (CD) investigations were carried out. Importantly, the presence of DMSO, even in traces, greatly affects the analysis, and this feature, in addition to the short stabilities of **3R, S**, limited the CD experi-
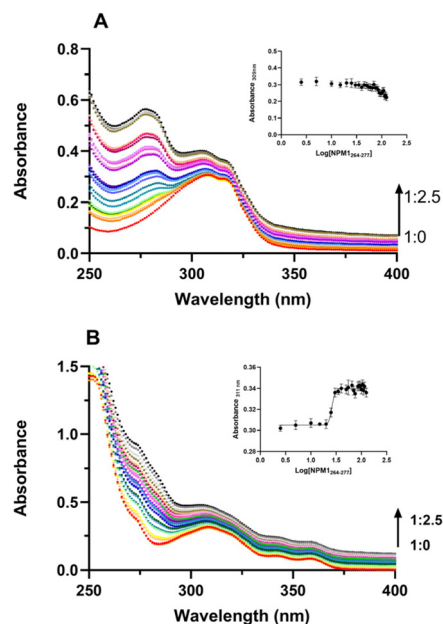
Fig. 4 UV-vis titration of compound **1** and **2** with NPM1$_{264-277}$. Absorption spectra of **1** (A) and **2** (B) upon the addition of increasing amount of NPM1$_{264-277}$. Arrows indicate the variation of the ratio complex : peptide. As insets UV intensities at indicated wavelengths *versus* log concentration of NPM1$_{264-277}$ are reported.

ments to water-soluble **1** and **2** complexes, only. The overlays of CD spectra of NPM1$_{264-277}$ alone and in the presence of metal complexes, at 1 : 1 ratio, recorded over a period of 12 h, are reported in Fig. 5. For NPM1$_{264-277}$ alone, a clear transition from a mixed α-helix and β-structure (Fig. 5A) toward a prevalent β-conformation is observable, as well as a decrease of Cotton effect due to aggregation, as previously reported.[38] The presence of **2** complex, already at t = 0 h, stabilized β-conformation leading to the highest β content at 3 h of analysis (Fig. 5C), as confirmed by deconvolution percentages of spectra reported in Table S1.† On the contrary, the sample of NPM1$_{264-277}$ + **1** exhibited a time-evolution of CD profile more similar to that of the peptide alone (Fig. 5B).

Effects of Pt complexes on the morphology of NPM1$_{264-277}$ fiber

To get insights into the effects of Pt-complexes on the morphology of the fibers derived from NPM1$_{264-277}$, scanning electron microscopy (SEM) experiments were carried out. Fibers of NPM1$_{264-277}$ in a previous SEM analysis, exhibited ~20 μm in diameter and ~1.3 mm in length.[38] Herein, compounds **1**, **2** and **3S** were added to freshly prepared solutions of NPM1$_{264-277}$ and after 2 h (for **3S**) and 4 h (for **1** and **2**) of incubation, the aggregates were analyzed. Compared to peptide alone, both the length and diameter of the aggregates were perturbed in the presence of metal complexes, as shown in Table 2. In detail, the presence of **2** caused a reduction of the diameter of the fiber (from ~20 μm in NPM1$_{264-277}$ alone to 8 μm; Fig. 6A–A″ and Table 2), while the addition of **3S**
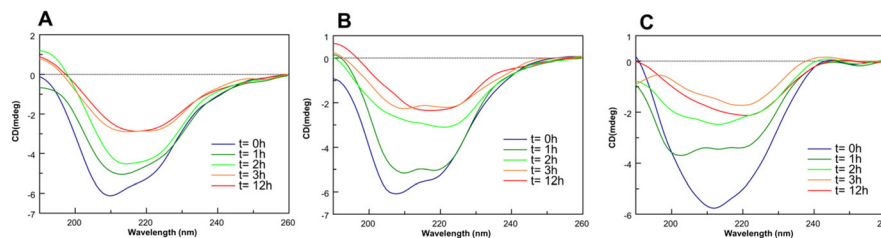
Fig. 5 Overlay of CD spectra of NPM1$_{264-277}$ (A) alone and incubated with **1** (B) and **2** (C), at 1 : 1 peptide: Pt(II) compound molar ratio.

Table 2 SEM analyses: average diameter and length of fibers obtained for NPM1$_{264-277}$ in the presence and in the absence of **2** and **3S** complexes

	Average diameter (μm)	Length (μm)
NPM1$_{264-277}$[a]	22 ± 5	1270
NPM1$_{264-277}$ + **2**	8 ± 3	900
NPM1$_{264-277}$ + **3S**	15 ± 2	500

[a] Ref. 38.

caused a marked reduction of the length dimension (from ~1.3 mm to ~0.5 mm; Fig. 6B–B″ and Table 2), besides to a slight thinning effect. On the contrary, the presence of **1** did not cause significant changes in the fiber, confirming its less modulating effect on the amyloid aggregation (Fig. S2†).

Charged Pt-complex directly interact with NPM1$_{264-277}$

On the basis of the greater effect exhibited by **2** with respect to **1** on the aggregation of NPM1-amyloid, the last series of experiments was performed only on **2** complex. NPM1$_{264-277}$ was incubated with **2** at two different times (0 h and 4 h, respectively) and the resulting mixtures were analyzed by electrospray ionization mass spectrometry (ESI-MS) (Fig. 7A t = 0 h; Fig. 7B t = 4 h). In the presence of **2**, the spectra showed the occurrence of peaks due to adducts between one peptide chain and one (#1) or two metal complexes (#2, #3; Table 3). In detail, the peak #1 (m/z 1080.483 u) showed a species corres-
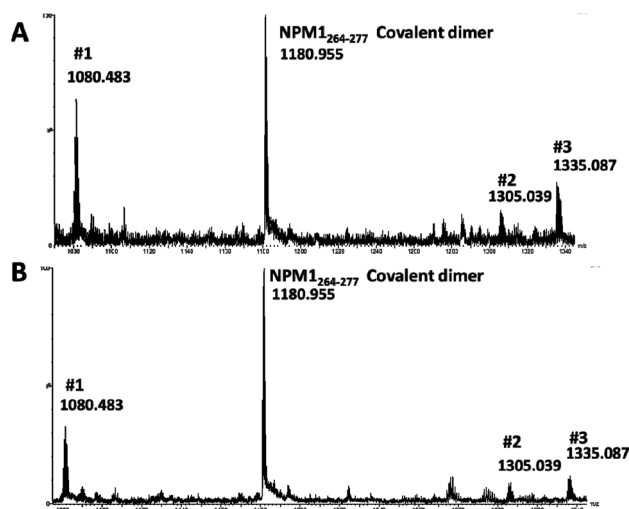

Fig. 7 **2** compound interacts with NPM1$_{264-277}$. ESI-MS spectra of NPM1$_{264-277}$ peptide incubated with **2** compound at (A) t = 0 h, and (B) t = 4 h.

ponding to the adduct with a 1 : 1 stoichiometry, in which the Pt-complex lost one Cl$^-$ and one NH$_3$ ligand. Instead, peaks #2 and #3 are attributed to adducts with a 1 : 2 stoichiometry, peptide: **2**: #2 is related to the adduct among one peptide chain and two **2** moieties lacking 3 × NH$_3$, while #3 corresponds to the #2 carrying one additional acetate ion, which is
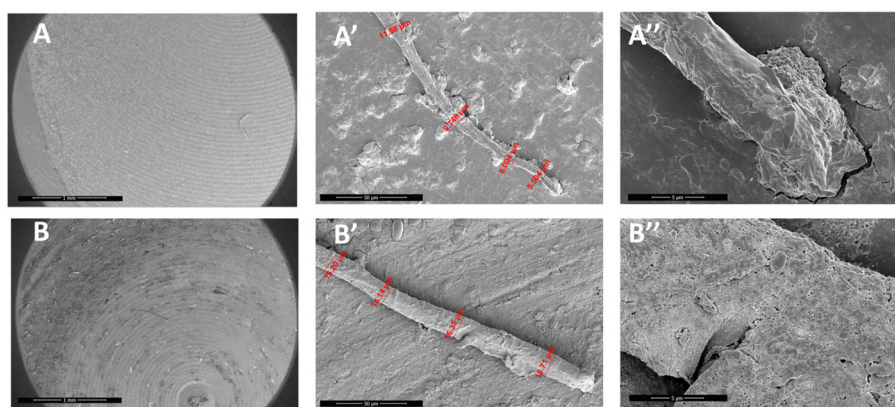

Fig. 6 Effects of Pt-complexes on amyloid fibers. SEM micrographs of (A–A″) NPM1$_{264-277}$ + **2**, (B–B″) NPM1$_{264-277}$ + **3S** at 1 : 5 ratio, at (A and B) 1 mm, (A′ and B′) 50 μm and (A″ and B″) 5 μm.

Table 3 Table of main ions formed by NPM1$_{264-277}$ with **2**. Experimental, theoretical mass and charge are reported for each adduct

Experimental conditions	Experimental m/z	Charge	Theoretical m/z	Description	
NPM1$_{264-277}$ + **2**, 0 h	1080.483	2	1081.63	NPM1$_{264-277}$ + **2**−1Cl$^-$−1 NH$_3$	#1
	1305.039	2	1305.26	NPM1$_{264-277}$ + 2 **2**−3 NH$_3$	#2
	1335.087	2	1335.773	**#2** + acetate	#3
	1180.955	3	1180.931	NPM1$_{264-277}$ covalent dimer	
NPM1$_{264-277}$ + **2**, 4 h	1080.483	2	1081.63	NPM1$_{264-277}$ + **2**−1Cl$^-$−1 NH$_3$	#1
	1305.039	2	1305.26	NPM1$_{264-277}$ + 2 **2**−3 NH$_3$	#2
	1335.087	2	1335.773	**#2** + acetate	#3
	1180.955	3	1180.931	NPM1$_{264-277}$ covalent dimer	

present in the buffer. As already reported,[19] the presence of Cys^{275}, allow the formation of dimeric forms of the amyloid peptide, already at $t = 0$.

Modelling studies of interaction complex 2 with NPM1$_{264-277}$

With the aim of identifying the most favorable metal-binding modes between NPM1$_{264-277}$ and the Pt complexes computational modelling studies were performed. Initial tests at the semi-empirical GFN2-xTB level[39] indicate that compound **2** binds preferentially to the deprotonated thiol side chain of Cys^{275}, with a binding energy more stable of ∼30 kJ mol^{-1} than any other available site. Possible cation–π interactions between the extended π-system of the ligand with Lys^{273} and Arg^{277} were evident. However, the flexible nature of the peptide means that such interactions may not persist, so we used molecular dynamics (MD) simulations to predict the conformations of the peptide with and without **2** bound. Over the course of 3 independent 100 ns simulations, metal-free monomeric NPM1$_{264-277}$ folds quickly and consistently into α-helical fold (Fig. S2 and S3†). Helices start to form within 10 ns and persist over the course of each simulation, albeit with some fluctuations to partially folded forms. Clustering procedure finds that the most populated cluster is a fully-folded α-helix, consisting of 19% of all frames recorded (Fig. 8A), and other clusters consisting of partially-folded helices (14 and 11%), all in agreement with the native secondary and tertiary structures of NPM1 protein.[40] Conformations adopted by a non-covalent dimer of NPM1$_{264-277}$ strongly depend on starting conformation: in parallel or crossed construction no clear secondary structure forms, and in some cases, the dimer dissociates. However, when constructed in antiparallel form from extended monomer conformation, MD simulation, quickly and consistently, brings to β-strand conformations (Fig. 8B).[41] These strands form almost instantly and encompass the entire length of each peptide chain, this self-interaction is at the basis of observed amyloid aggregation of the sequence NPM1$_{264-277}$.[16]

The presence of **2** bound to Cys^{275} drastically changes the conformational preferences of both monomer and dimer. The Pt-bound monomer (Fig. 8C) exhibits almost no helical character indeed the dictionary of protein secondary structure (DSSP) algorithm identifying only turn and bend elements[42] suggesting that the presence of the large Pt complex disrupts the helical organization of the isolated peptide. Similarly, the anti-parallel dimer appears strongly inhibited by the binding
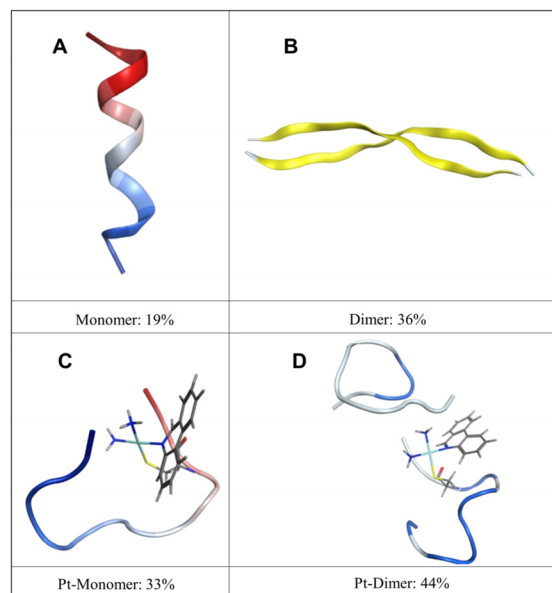

Fig. 8 Most populated clusters from 3 independent 100 ns simulations. (A) metal-free monomer; (B) metal-free non-covalent anti-parallel dimer; (C) monomer peptide : **2**; (D) dimer peptide : **2** adducts. Monomer is colored from N-terminus (blue) to C-terminus (red), while dimers are colored according to secondary structure (yellow = β-strand, blue = turn).

of **2** (Fig. 8D). In this case, some recorded frames contain β-strands, but these are smaller and shorter-lived than in the metal-free case. The maximum strand content is 22% of all recorded frames and is found for Phe^{268} of chain A and Phe^{276} of chain B. Closer analysis indicates the occurrence of several non-covalent interactions between **2** and the peptide chain in addition to the coordination bond to Cys^{275}. These connections include C–H⋯π interactions between Lys and the aromatic ligand of **2**, as well as hydrogen bonds from ammine ligands to backbone nitrogens of Val, Glu and Arg. The lack of a precise agreement between the ESI† data and the MD data is due to different phases, gas and aqueous buffer, and ratios of peptide to **2** complex.

Conclusions

Platinum-based therapeutics are widely used in a variety of chemotherapy regimens and studies aimed to deepen their

MOAs demonstrated that some of them are able to induce ribosome biogenesis stress pathway. In detail phenanthriplatin, which is a monofunctional Pt(II) compound, demonstrated the ability to relocalize NPM1[43] indicating that the spatial orientation and/or hydrophobicity of aromatic ring around metal ion can finely tune the cytotoxic effects of this important class of anticancer agents.[44] Much more recent is the interest in the ability of Pt-anticancers to interact with amyloid proteins and peptides[45] mainly through a coordinative mechanism often with concomitant interactions as electrostatic attraction, hydrogen bonding and van der Waals force[46] as well as π–π stacking among amino acids side chains and planar aromatic ligands. In the present study we have investigated the abilities of several Pt-complexes to impede fibril formation of amyloidogenic peptides reported in Table 1. Although the interaction between Pt complexes and amyloids is relatively weak[47] the coordination of these compounds to peptides remarkably changes the aggregation behavior of the amyloid peptides and among studied Pt-complexes phenanthriplatin, compound 2 (Fig. 1), demonstrated the most active. We propose that this difference may be due to a greater π-stacking contribution to the inhibitory mechanism of $NPM1_{264-277}$ exerted by 2, which bears a phenanthridine ligand. Indeed, the aromatic core constituted by $Phe^{268,276}$ and Tyr^{271} residues in NPM1 plays a crucial role in the self-aggregation mechanism of this amyloid model.[41] ThT-time courses, registered both upon the addition of the Pt compounds to freshly prepared samples or to soluble amyloid aggregates, indicated that 2 is very efficient to inhibit the fibrillation and to alter the particle sizes of peptide aggregates as clearly demonstrated, by means of SEM, on the morphology of aggregates. Other investigations demonstrated that the ligand configuration is a crucial factor in modulatory effect on amyloid fibrillation, which severely affects the binding patterns and sites of Pt-inhibitors. The MS analysis provided evidences for the formation of different types of adducts, all implying the binding of compound 2 to $NPM1_{264-277}$ through a common ligands' release process, with the retention of phenanthroline and the loss of the chlorine and ammonia, even if with different stoichiometries. CD studies indicated that 2 increased and stabilized the β-content of the amyloid peptide in early stages of aggregation and MD simulations indicated in the Cys residue the most involved in the coordination of metal center, with additional π–cation interactions and that the binding to 2 strongly affects the conformation of the peptide chain.

In conclusion this research provides critical information on the inhibition and disaggregation of amyloid fibrillation by phenanthroline-based metal complexes with impact on the biomedical value of clinical platinum drugs against amyloid diseases.

Author contributions

S. L. M. synthesized the peptide and performed fluorescence, UV and CD studies; V. M. and M. M. performed ESI-experiments;† V. R. did SEM assays; M. R. and E. G. synthesized and characterized the metal complexes; J. A. P. performed MD experiments; D. M. designed the concept, supervised the experiments and wrote the manuscript. All authors have read and approved the final version of the manuscript.

Conflicts of interest

The authors declare no competing interests.

Acknowledgements

References

1 G. Son, B. I. Lee, Y. J. Chung and C. B. Park, *Acta Biomater.*, 2018, **67**, 147–155.

2 I. Yousuf, M. Bashir, F. Arjmand and S. Tabassum, *Coord. Chem. Rev.*, 2021, **445**, 214104.

3 M. A. Telpoukhovskaia and C. Orvig, *Chem. Soc. Rev.*, 2013, **42**, 1836–1846.

4 C. Soto and S. Pritzkow, *Nat. Neurosci.*, 2018, **21**, 1332–1340.

5 T. D. Samdin, A. G. Kreutzer and J. S. Nowick, *Curr. Opin. Chem. Biol.*, 2021, **64**, 106–115.

6 K. J. Barnham, V. B. Kenche, G. D. Ciccotosto, D. P. Smith, D. J. Tew, X. Liu, K. Perez, G. A. Cranston, T. J. Johanssen and I. Volitakis, *Proc. Natl. Acad. Sci. U. S. A.*, 2008, **105**, 6813–6818.

7 K. D. Mjos and C. Orvig, *Chem. Rev.*, 2014, **114**, 4540–4563.

8 M. Van Beusichem and N. Farrell, *Inorg. Chem.*, 1992, **31**, 634–639.

9 F. Gumus, G. k. e. Eren, L. Açık, A. Celebi, F. Ozturk, S. u. k. Yılmaz, R. I. Sagkan, S. Gur, A. Ozkul and A. Elmalı, *J. Med. Chem.*, 2009, **52**, 1345–1357.

10 N. A. Al-Masoudi, B. H. Abdullah, A. H. Essa, R. Loddo and P. LaColla, *Arch. Pharm.*, 2010, **343**, 222–227.

11 I. Sasaki, C. Bijani, S. Ladeira, V. Bourdon, P. Faller and C. Hureau, *Dalton Trans.*, 2012, **41**, 6404–6407.

12 F. Collin, I. Sasaki, H. Eury, P. Faller and C. Hureau, *Chem. Commun.*, 2013, **49**, 2130–2132.

13 T. G. Chan, C. L. Ruehl, S. V. Morse, M. Simon, V. Rakers, H. Watts, F. A. Aprile, J. J. Choi and R. Vilar, *Chem. Sci.*, 2021, **12**, 9485–9493.

14 G. Gong, J. Xu, X. Huang and W. Du, *JBIC, J. Biol. Inorg. Chem.*, 2019, **24**, 179–189.

15 R. Cukalevski, B. Boland, B. Frohm, E. Thulin, D. Walsh and S. Linse, *ACS Chem. Neurosci.*, 2012, **3**, 1008–1016.

16 S. La Manna, M. Leone, I. Iacobucci, A. Annuziata, C. Di Natale, E. Lagreca, A. M. Malfitano, F. Ruffo, A. Merlino, M. Monti and D. Marasco, *Inorg Chem*, 2022, **61**, 3540–3552.

17 C. Di Natale, P. L. Scognamiglio, R. Cascella, C. Cecchi, A. Russo, M. Leone, A. Penco, A. Relini, L. Federici, A. Di Matteo, F. Chiti, L. Vitagliano and D. Marasco, *FASEB J.*, 2015, **29**, 3689–3701.

18 D. Florio, M. Cuomo, I. Iacobucci, G. Ferraro, A. M. Mansour, M. Monti, A. Merlino and D. Marasco, *Pharmaceuticals*, 2020, **13**, 171.

19 S. La Manna, V. Roviello, F. Napolitano, A. M. Malfitano, V. Monaco, A. Merlino, M. Monti, K. Kowalski, Ł. Szczupak and D. Marasco, *Inorg. Chem.*, 2023, **62**, 10470–10480.

20 M. M. Patino, J.-J. Liu, J. R. Glover and S. Lindquist, *Science*, 1996, **273**, 622–626.

21 J. R. Glover, A. S. Kowal, E. C. Schirmer, M. M. Patino, J.-J. Liu and S. Lindquist, *Cell*, 1997, **89**, 811–819.

22 M. Balbirnie, R. Grothe and D. S. Eisenberg, *Proc. Natl. Acad. Sci. U. S. A.*, 2001, **98**, 2375–2380.

23 S. La Manna, D. Florio, I. Iacobucci, F. Napolitano, I. D. Benedictis, A. M. Malfitano, M. Monti, M. Ravera, E. Gabano and D. Marasco, *Int. J. Mol. Sci.*, 2021, **22**, 3015.

24 G. Y. Park, J. J. Wilson, Y. Song and S. J. Lippard, *Proc. Natl. Acad. Sci. U. S. A.*, 2012, **109**, 11987–11992.

25 D. R. Roe and T. E. Cheatham III, *J. Chem. Theory Comput.*, 2013, **9**, 3084–3095.

26 S. Bombard, M. B. Gariboldi, E. Monti, E. Gabano, L. Gaviglio, M. Ravera and D. Osella, *JBIC, J. Biol. Inorg. Chem.*, 2010, **15**, 841–850.

27 E. Gabano, S. Gama, F. Mendes, M. B. Gariboldi, E. Monti, S. Bombard, S. Bianco and M. Ravera, *JBIC, J. Biol. Inorg. Chem.*, 2013, **18**, 791–801.

28 D. Case, D. Cerutti, T. Cheatham, T. Darden, R. Duke, T. Giese, H. Gohlke, A. Goetz, D. Greene and N. Homeyer, *AMBER* 2016, University of California, San Francisco.

29 J. A. Maier, C. Martinez, K. Kasavajhala, L. Wickstrom, K. E. Hauser and C. Simmerling, *J. Chem. Theory Comput.*, 2015, **11**, 3696–3713.

30 P. Li and K. M. Merz Jr., *J. Chem. Inf. Model.*, 2016, 599–604.

31 J. M. Seminario, *Int. J. Quantum Chem.*, 1996, **60**, 1271–1277.

32 C. Di Natale, S. La Manna, A. M. Malfitano, S. Di Somma, D. Florio, P. L. Scognamiglio, E. Novellino, P. A. Netti and D. Marasco, *Biochim. Biophys. Acta, Proteins Proteomics*, 2019, **1867**, 637–644.

33 T. Tanaka, V. V. Betkekar, K. Ohmori, K. Suzuki and H. Shigemori, *Pharmaceuticals*, 2021, **14**, 1118.

34 G. Arena, G. Calogero, S. Campagna, L. Monsù Scolaro, V. Ricevuto and R. Romeo, *Inorg. Chem.*, 1998, **37**, 2763–2769.

35 E. L. McInnes, R. Farley, C. Rowlands, A. Welch and L. Yellowlees, *J. Chem. Soc., Dalton Trans.*, 1999, 4203–4208.

36 V. X. Jin and J. D. Ranford, *Inorg. Chim. Acta*, 2000, **304**, 38–44.

37 M. Imran, Z. ur Rehman, G. Hogarth, D. A. Tocher, I. S. Butler, F. Bélanger-Gariepy and T. Kondratyuk, *Dalton Trans.*, 2020, **49**, 15385–15396.

38 D. Florio, V. Roviello, S. La Manna, F. Napolitano, A. M. Malfitano and D. Marasco, *Bioorg. Chem.*, 2022, **127**, 106001.

39 C. Bannwarth, S. Ehlert and S. Grimme, *J. Chem. Theory Comput.*, 2019, **15**, 1652–1671.

40 C. G. Grummitt, F. M. Townsley, C. M. Johnson, A. J. Warren and M. Bycroft, *J. Biol. Chem.*, 2008, **283**, 23326–23332.

41 A. Russo, C. Diaferia, S. La Manna, C. Giannini, T. Sibillano, A. Accardo, G. Morelli, E. Novellino and D. Marasco, *Biochim. Biophys. Acta, Proteins Proteomics*, 2017, **1865**, 176–185.

42 W. G. Touw, C. Baakman, J. Black, T. A. Te Beek, E. Krieger, R. P. Joosten and G. Vriend, *Nucleic Acids Res.*, 2015, **43**, D364–D368.

43 C. E. McDevitt, M. V. Yglesias, A. M. Mroz, E. C. Sutton, M. C. Yang, C. H. Hendon and V. J. DeRose, *JBIC, J. Biol. Inorg. Chem.*, 2019, **24**, 899–908.

44 Z. Deng and G. Zhu, *Curr. Opin. Chem. Biol.*, 2023, **74**, 102303.

45 T. Zheng, Y. Huo, Y. Wang and W. Du, *J. Inorg. Biochem.*, 2022, **237**, 111989.

46 J. Zhao, K. Li, K. Wan, T. Sun, N. Zheng, F. Zhu, J. Ma, J. Jiao, T. Li and J. Ni, *Angew. Chem., Int. Ed.*, 2019, **58**, 18032–18039.

47 G. Ma, E. Wang, H. Wei, K. Wei, P. Zhu and Y. Liu, *Metallomics*, 2013, **5**, 879–887.